The Thesis Committee for Patrick Joseph Crowley Certifies that this is the approved version of the following Thesis:

Diffusional lithium trapping as a failure mechanism of aluminum foil anodes in lithium-ion batteries

APPROVED BY
SUPERVISING COMMITTEE:

Arumugam Manthiram, Supervisor

Venkat Subramanian

Diffusional lithium trapping as a failure mechanism of aluminum foil anodes in lithium-ion batteries

by

Patrick Joseph Crowley

Thesis

Presented to the Faculty of the Graduate School of

The University of Texas at Austin

in Partial Fulfillment

of the Requirements

for the Degree of

Master of Science in Engineering

The University of Texas at Austin

August 2022

Acknowledgements

I would like to thank Professor Arumugam Manthiram for his financial support and mentorship during my time in his lab as a graduate researcher. I would also like to thank Professor Venkat Subramanian for his guidance on my research projects. I am extremely grateful to my peers in the Manthiram lab for their friendship and support throughout my time at UT Austin. I would like to thank Shyam Sharma, Joe Darga, Richard Sim, Steven Lee, Kevin Scanlan, and Brian Heligman for their kindness and guidance. Thanks also to my partner and best friend, Rachel Joachimi, for her support towards this endeavor. Lastly, I wish to thank my parents, Patrick and Sandy Crowley, for their constant encouragement and for their endless love.

Abstract

Diffusional lithium trapping as a failure mechanism of aluminum foil anodes in lithium-ion batteries

Patrick J. Crowley, M.S.E.
The University of Texas at Austin, 2022

Supervisor: Arumugam Manthiram

Aluminum foils are an appealing anode for lithium-ion batteries due to their high capacity and low-cost, but their viability has been limited due to poor cyclability arising from pulverization and solid-electrolyte interphase growth. We show in this thesis that significant capacity degradation of aluminum foil anodes during electrochemical cycling also occurs due to diffusional lithium trapping. Scanning electron microscopy of cross-sectioned, cycled foils in the delithiated state reveals large regions of β-LiAl that are passivated by a surface layer of α-Al, which has poor Li^+ diffusivity. It is found that lithium diffusion occurs preferentially along the β-LiAl grain boundaries, so the grain structure after initial lithiation significantly affects the trapping behavior. Diffusional lithium trapping is exacerbated by both higher delithiation rates and higher areal capacity, presenting a challenge towards commercialization of aluminum foil anodes. We further

demonstrate that diffusional trapping in aluminum foil anodes can be mitigated through alloy design, with the addition of 2 – 3 wt.% Li yielding improved first cycle efficiency, and the addition of 1 wt.% Si yielding improved cycle life. These results provide a mechanistic understanding of diffusional lithium trapping in aluminum foil anodes and highlight compositional design of alloys as a promising strategy to overcome it.

Table of Contents

List of Figures

Chapter 1: Introduction

1.1 Motivation

A climate crisis arising from global temperature rise caused by human activities has been detrimentally impacting living systems for decades. Symptoms of the climate crisis, such as extreme weather events, oceanic acidification, and widespread loss of biodiversity, are already exacerbating global economic disparity and causing massive migrations among the human population. In order to prevent a worsening of the climate crisis, a rapid shift away from human activities that emit greenhouse gases on a massive scale must take place. Clean energy technologies such as solar and wind power for electricity generation and electric vehicles for transportation have potential to replace fossil fuels and decrease the greenhouse gas emissions by humans, curbing the adverse impact on the Earth's climate. Intermittent renewable energy sources and electric vehicles both require electrochemical energy storage in the form of batteries to function properly in the modern world.

1.2 Improving Lithium-ion Battery Anodes

Lithium-ion batteries (LIBs) are essential for the world to transition towards sustainable technologies, such as electric vehicles and use of intermittent renewable energy sources. LIB technology has taken massive strides forward in terms of sustainability, cost, lifetime, and energy density, but there is still room for improvement in all of these spaces.[1-4] While graphite has been the anode material of choice due to its well-rounded performance characteristics, further increases in volumetric capacity and fast charging capability are needed.[5,6] An ideal LIB anode material must simultaneously improve energy density and charging rate without sacrificing lifetime, safety, material cost, or sustainability.

Alloying anodes (*e.g.*, Si, Sn, Al, etc.) are a promising alternative to intercalation anodes like graphite, as they offer much higher gravimetric and volumetric capacity, while the slightly higher operating voltage reduces the risk of lithium plating during fast charging.[7,8] They can also improve upon the material-level sustainability and cost compared to graphite.[4] Alloy anodes are particularly attractive in a foil electrode geometry, since fully-dense foils yield improved volumetric capacity and lower processing cost compared to the more commonly studied porous electrodes fabricated through slurry coating. Aluminum and tin are the most suitable active materials for high-capacity foil anodes, but the high cost and restricted supply of Sn is a barrier to commercialization.[9] Despite their low technological maturity, aluminum foil anodes have the potential to revolutionize LIB technology due to their high theoretical capacity (993 mAh g^{-1} for α-Al → β-LiAl),[7,8,10] extremely low material cost (< 1 \$ kWh^{-1}), high material abundance (2nd most abundant metal),[11] and sustainability.[4,12]

However, the main shortcoming of alloying anodes is their insufficient cycle life, which has so far prevented them from replacing graphite in commercial LIBs. It is generally understood that the rapid capacity fade of alloying anodes during electrochemical cycling results from their massive volume changes associated with lithium alloying and de-alloying.[13-16] This causes mechanical pulverization of the active material, leading to loss of lithium inventory and electronic isolation of active material particles due to continued solid-electrolyte interphase (SEI) growth. Thus, the primary research focus has been understanding and solving failure mechanisms related to volume changes and interfacial stability.[17,18] Many approaches have been demonstrated to mitigate these failure mechanisms, with a range of success in both foil format[19,20] and in the slurry-casted nanoparticle format.[21]

Aluminum has a markedly lower volume expansion (96% for α-Al → β-LiAl) relative to most other alloying anodes (*e.g.*, 280% for Si → $Li_{15}Si_4$, and 310% for Sn → $Li_{22}Sn_5$),[8] which should lead to less mechanical pulverization during cycling. However, despite this reduction in the supposed root cause of capacity fade, aluminum still exhibits much worse cycle life than other alloying anodes, especially in a foil electrode geometry. For example, sustained coulombic efficiency (CE) of < 90% is commonly reported, leading to cell failure after only a few cycles.[10,12,22] It has been suggested that this rapid capacity fade could result from the poor electronic conductivity and irreversible lithium consumption of Al_2O_3 surface layers.[15] However, while these mechanisms may be prominent in nanosized Al (*e.g.*, nanowires), they should not be significant in foils due to their extremely low surface area. Another possible failure mechanism is diffusion-controlled lithium trapping, which has been shown to occur in both silicon and tin anodes.[5,23,24] This behavior is ascribed to the differences in lithium diffusivities among the lithium-rich and lithium-poor phases formed during alloying/dealloying. If the lithium-poor phases formed on the active material surface during delithiation have low lithium diffusivity, then lithium diffusion from the unreacted lithium-rich phases can be significantly impeded. This diffusional trapping mechanism is expected to be more prominent in foil anodes, which have lower surface area and longer diffusion path lengths compared to nano- or micro-particle alloying anodes.

The alloying/dealloying reactions of aluminum occur via a two-phase reaction between α-Al and β-LiAl, resulting in a flat voltage profile.[9] Due to the vast difference in lithium diffusivities between these two phases, diffusional lithium trapping is expected to occur in aluminum anodes, as first discussed by Owen *et al.*[25] The lithium diffusivity of α-Al is ~ 10^{-11} cm^2 s^{-1}, while the diffusivity of β-LiAl is as high as 10^{-8} to 10^{-9} cm^2 s^{-1}.[26-28] Upon delithiation, the two-phase transformation could result in the formation of an α-Al layer on the surface which, due to its low

diffusivity, would prevent further delithiation once it reaches a sufficient thickness. Diffusional lithium trapping in aluminum anodes has been investigated by some groups, but remains poorly understood as the conclusions of these reports have been contradictory.[29-32] These investigations have generally used aluminum thin films or nanorods, in which other mechanisms of degradation may be more prominent than diffusional trapping.[29,30] Some of these reports have also neglected the possibility that the existence of β-LiAl in fully delithiated aluminum electrodes could be due to electronic isolation through SEI growth or mechanical degradation, rather than diffusional trapping.[31,33] Overall, clear evidence of diffusional lithium trapping in aluminum foil anodes has not been demonstrated in the literature, and it remains unclear to what extent this mechanism affects the first cycle columbic efficiency and cycle life of aluminum foil anodes.

In this work, we demonstrate that diffusional lithium trapping is a significant source of capacity fade in aluminum foil anodes by employing limited-lithium inventory (LLI) electrochemical cycling, cross-sectional scanning electron microscopy (SEM), and X-ray diffraction (XRD). Through the analysis of the foil microstructure during the first delithiation, clear evidence for the diffusional lithium trapping mechanism is presented. First cycle efficiency and cycle life of aluminum foil anodes is evaluated at various areal capacities and delithiation rates to understand how diffusional trapping affects the performance under practically relevant conditions. A series of aluminum alloys containing silicon and/or lithium are also investigated, which show improvements to first cycle efficiency and/or cycle life compared to pure Al foils.

Chapter 2: Experimental Methods

2.1 Material Synthesis

Aluminum foils were prepared with conventional metallurgical techniques, with the following compositions given by weight %: Al, Al-Li ($Al_{97.0}Li_{3.0}$), Al-Si ($Al_{99.0}Si_{1.0}$), and Al-Li-Si ($Al_{97.0}Li_{2.0}Si_{1.0}$). Aluminum shots (99.99%, Belmont Metals Inc.) and silicon pieces (99.95%, Sigma-Aldrich) were used as-received, while lithium-metal rods (99.9%, Sigma-Aldrich) were melted, scraped of surface impurities, and recast to ensure the highest purity. For each alloy, the metals were weighed to achieve the desired composition, and then melted in graphite crucibles at 760 °C in a box furnace within an argon-filled glovebox. The melts were stirred to ensure homogeneity and then cast into graphite molds, giving ingots with dimensions of 50 mm × 20 mm × ~ 15 mm. The ingots were sanded and were then repeatedly passed through an electric rolling mill (Duston TUI 130) until the thickness was reduced to ~ 40 μm. The foils were punched to ½" diameter disks for electrochemical characterization.

2.2 Battery Assembly and Electrochemical Characterization

Electrochemical characterization was conducted in CR 2032 coin cells with a Li-metal counter electrode. Each cell consisted of a 1/2" diameter foil electrode, a 3/4" Celgard 2325 separator, a 5/8" Li-metal chip (MTI, 0.5mm thick), a 5/8" stainless steel spacer (0.5mm thick), and a 1/2" diameter Ni foam to apply stack pressure. The electrolyte was LP57 (1.0 M $LiPF_6$ in 3 : 7 by weight of ethylene carbonate and ethyl methyl carbonate) mixed with 3 wt% fluoroethylene carbonate. Coin cells were assembled inside an argon-filled glovebox. All electrochemical tests were performed at room temperature with an Arbin BT-2043 battery tester. Cycle life testing was conducted with a lithium-limited inventory (LLI) cycling protocol, in which a capacity cutoff is used for lithiation and a voltage cutoff (1.5 V vs. Li/Li^+) is used for delithiation. For the first cycle,

the lithiation capacity cutoff was set to the desired areal capacity, while for all subsequent cycles, the lithiation capacity cutoff was set to the delithiation capacity of the previous cycle. The standard cycling protocol included an initial lithiation capacity of 2.0 mAh cm^{-2}, two formation cycles at a current of 0.2 mA cm^{-2} (C/10), followed by cycling at a current of 0.67 mA cm^{-2} (C/3) until the cells either failed or reached 200 cycles. For testing at different areal capacities, a current of 0.67 mA cm^{-2} was used for both lithiation and delithiation. For testing at different delithiation rates, the current for lithiation was fixed at 0.67 mA cm^{-2} (C/3).

2.3 Material Characterization

Prior to analysis, the cycled foils were prepared by disassembling cycled coin cells in a glovebox and rinsing several times with acetonitrile to remove residual electrolyte. For cross-sectioning, the foils were then cut down at the center with a razor blade and mounted on a small piece of silicon wafer with carbon tape. A Hitachi IM4000C Broad Beam Ion Milling System directly attached to a glovebox was then used (5 kV for 40 minutes) to obtain smooth cross-sections from the center of the cycled foils. The cross-sectioned foils were imaged with the backscattered electron detector in an FEI Quanta 650 ESEM with a 20 keV acceleration voltage. X-ray diffraction (XRD) was conducted on both pristine and cycled foils with a Rigaku Miniflex 600 diffractometer. Diffraction patterns were collected over a 2θ range of $20-80°$ at a scan rate of 1.25°/min. Pristine foils were mounted directly onto a glass sample holder, while cycled foils were mounted in an air-sensitive XRD sample holder with a Kapton window.

Chapter 3: Results and Discussion

3.1 Identifying the mechanism of diffusional lithium trapping in aluminum foil anodes

LLI cycling was employed to test the cycle life of aluminum foil anodes under conditions, which accurately reflect full-cell performance, as was shown in a previous work.[14] The Al foil anodes exhibit rapid capacity fade, with only < 75% retained capacity after 5 cycles and < 50% retained capacity after 15 cycles (Figure 1a). The first cycle efficiency of 90.1% is still very high compared to most alloying anodes, and comparable to that of graphite anodes. Cycled electrodes were extracted from half cells between 1 to 4 cycles (after delithiation to 1.5 V vs. Li/Li^+), and the phase composition was characterized with XRD (Figure 1b). After only one cycle, the XRD pattern shows peaks corresponding to β-LiAl, and these peaks remain similar in magnitude after 4 cycles. The presence of LiAl after the first delithiation indicates that the first cycle capacity loss cannot

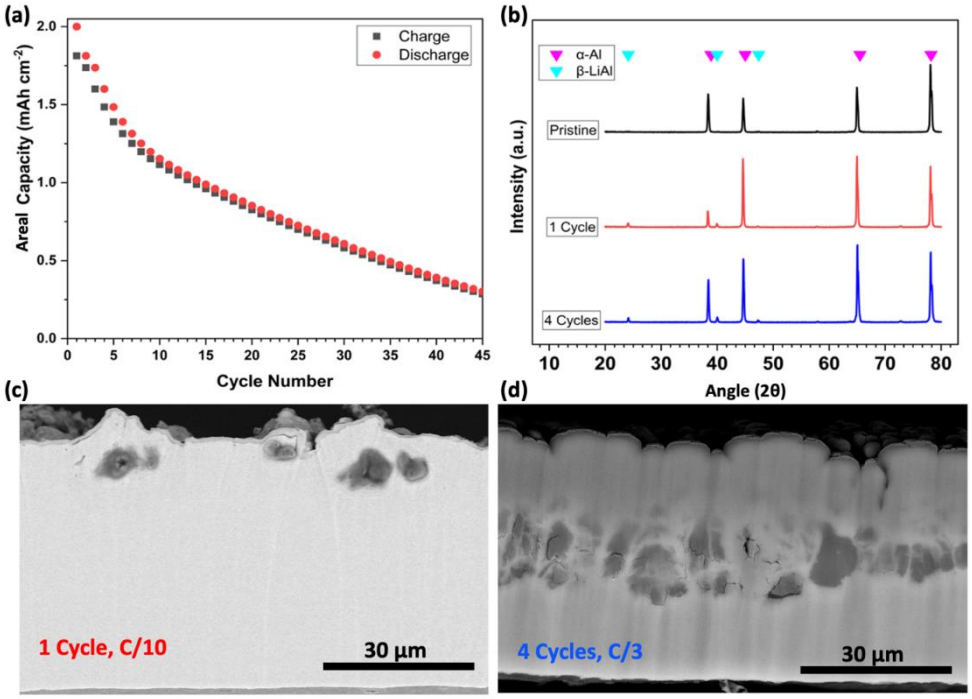

Figure 1: Electrochemical cycling data and post-mortem characterization of aluminum foil anodes between 1 – 4 cycles. **(a)** Areal charge and discharge capacity versus cycle number of an aluminum foil anode cycled following the standard protocol. **(b)** XRD patterns of pristine and cycled aluminum foils. **(c-d)** Cross-sectional BEIs collected after the **(c)** 1st cycle at a C/10 rate and **(d)** 4th cycle at a C/3 rate

be fully attributed to SEI formation.

The residual LiAl could either be ionically isolated from the electrolyte via a diffusional trapping mechanism, or electronically isolated from the current collector due to pulverization and/or SEI growth, but these mechanisms have not yet been distinguished.[33] To determine which of these mechanisms is dominant, the morphology of LiAl in the cycled foils was characterized with scanning electron microscopy (SEM) with a backscattered electron detector, which provides contrast based on atomic number. In the backscattered electron images (BEI), the LiAl regions appear darker due to the lower average atomic number compared to Al. After one cycle, small regions of LiAl are observed below the foil surface, which are fully covered by a layer of Al (Figure 1c). Between 2 – 4 cycles, the regions of LiAl grow larger in size and are observed deeper in the foil (Figures 1d and S1). After 4 cycles, the foil is still highly dense and there does not appear to be significant mechanical degradation, although small cracks are observed near the LiAl regions. Given that both phases are highly electronically conductive and the LiAl is in direct contact with the unreacted Al, which acts as a current collector, electronic isolation of the LiAl is not expected to occur.[34] Therefore, the rapid capacity loss within the first few cycles can mostly be attributed to diffusional trapping resulting from the passivation of LiAl by a surface layer of Al.[23,24] However, it is also possible that cracking in the interior of the foil could contribute to diffusional trapping by disrupting the solid-state diffusion pathways.

In order to better understand the mechanism of diffusional lithium trapping in aluminum foil anodes, the morphological evolution during the first cycle (C/3 rate at 2.0 mAh cm^{-2}) was investigated with SEM (Figure 2). Electrodes were extracted from half cells after different degrees of delithiation and then cross sectioned for imaging. After the initial lithiation, the LiAl layer has a uniform thickness of ~ 15 μm and exhibits a columnar grain structure, consistent with previous

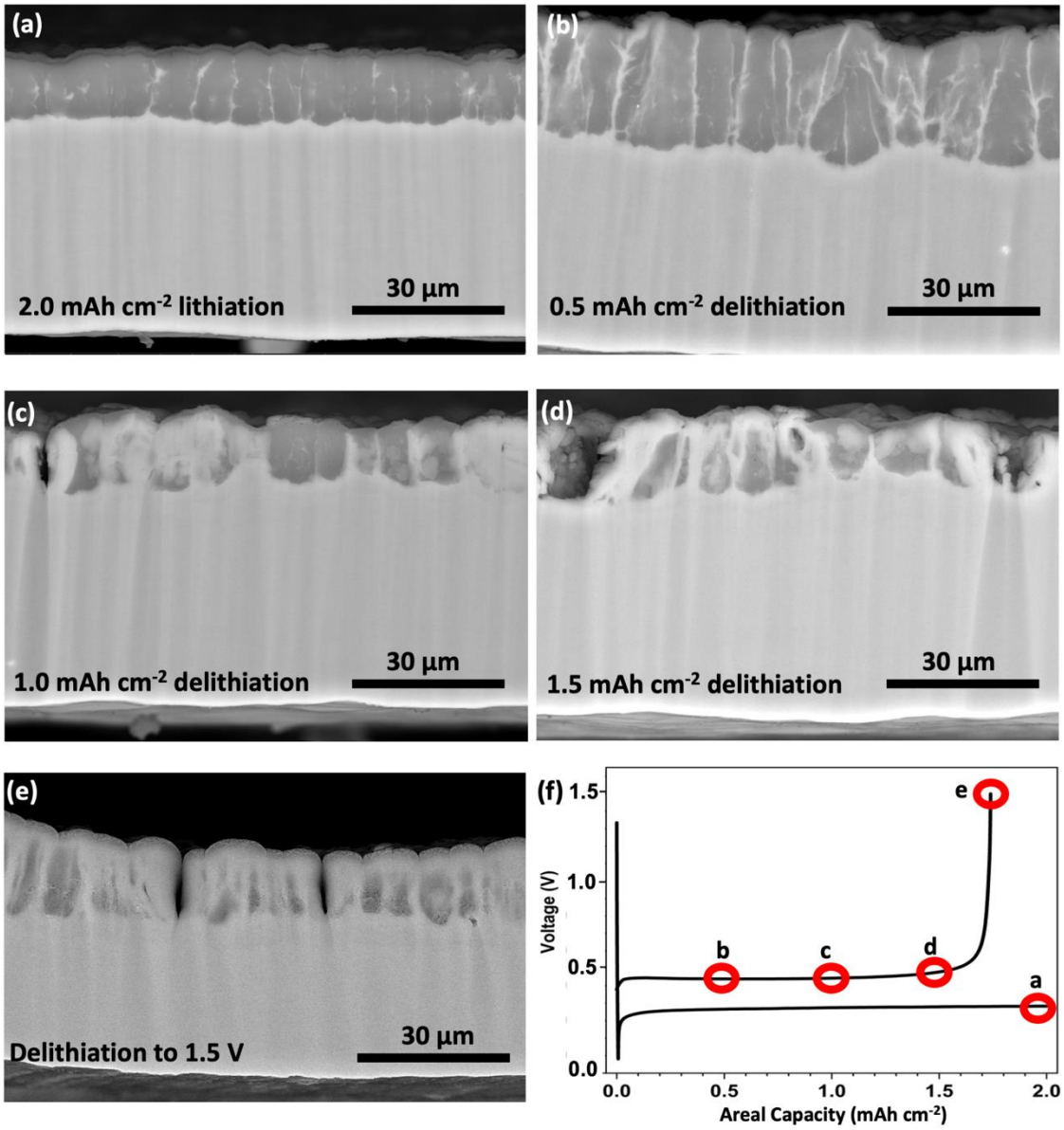

Figure 2: Evolution of the foil morphology during the 1st delithiation at a C/3 rate. **(a-e)** Cross-sectional BEIs of aluminum foil anodes stopped at 0.5 mAh cm^{-2} increments during the 1st delithiation. **(f)** Representative voltage versus capacity plot for the 1st cycle, showing the cycling history corresponding to each image.

results (Figure 2a).[35,36] The LiAl grains are between 5 – 10 µm wide, and thin regions of Al (< 1 µm) are visible at the grain boundaries, although the thickness of these regions is highly variable. At the beginning of delithiation (≤ 0.5 mAh cm^{-2}), the reaction occurs mainly at the grain

boundaries rather than at the surface of the foil. This is evidenced by the increased width of Al regions between the LiAl grains and the absence of Al on the foil surface (Figure 2b). This preferential reaction at the LiAl grain boundaries can be attributed to presence of Al, as the two-phase reaction can proceed without requiring nucleation of the α-Al phase, unlike the surface where no Al is initially present.[36] Solid-state diffusion in metals is typically enhanced at grain boundaries, so the phase boundaries between α-Al and β-LiAl along the columnar grains likely provide rapid lithium diffusion pathways through the thickness of the foil.[37]

As the delithiation proceeds to 1.0 mAh cm^{-2}, there is evidence of significant heterogeneity within the foil, where some LiAl grains have been fully delithiated and others remain mostly unreacted (Figure 2c). This behavior likely arises from the observed heterogeneity in the thickness of the Al regions at the grain boundaries after the initial lithiation. Since nucleation of α-Al at the LiAl grain boundaries should be kinetically unfavorable compared to the growth of pre-existing Al regions, the grain boundaries with thicker and/or more continuous Al regions likely react more quickly.[38] There are also large vertical cracks between some of the grains, which propagate through the entire thickness of the LiAl layer, with a similar morphology to the "mud-cracking" observed from the surface of other alloy electrode systems.[4,39] This cracking likely results from the anisotropic contraction of the foil due to the preferential delithiation at the grain boundaries and may be exacerbated by the observed reaction heterogeneity, which is expected to concentrate the stress into localized areas. Over numerous cycles, this cracking is expected to cause capacity degradation due to exposure of new surface area for SEI formation, as well as disruption of the electronic conduction pathways.[40] However, these cracks also locally reduce the solid-state diffusion path length, which should mitigate diffusional lithium trapping. Indeed, significantly less residual LiAl is observed after delithiation at the grains directly adjacent to cracks.

Near the end of delithiation, a continuous Al layer begins to grow on the surface, which blocks access of the electrolyte to the rapid diffusion pathway at the grain boundaries (Fig 2d-e and S2). After a full delithiation to 1.5 V, the irreversible capacity is 0.262 mAh cm^{-2}, corresponding to a first cycle efficiency of 87%. The remaining LiAl regions are mostly at the center of the initial grains, and are covered on all sides by a thin layer of α-Al, which has a uniform thickness of about 3 – 5 μm. Overall, these observations confirm that diffusional lithium trapping is a significant failure mechanism of aluminum foil anodes, and it occurs due to a passivation of β-LiAl by a surface layer of α-Al, following the preferential delithiation along the β-LiAl grain boundaries. .

3.2 Consequences of diffusional trapping on first cycle efficiency and cycle life

Diffusional lithium trapping is a kinetic phenomenon, so it should be exacerbated by both higher delithiation rate and higher areal capacity. The delithiation current density was varied between 0.2 mA cm^{-2} (C/10) and 2.0 mA cm^{-2} (1C) to understand the effect of delithiation rate on first cycle efficiency and cycle life (Figure 3a,c,d). The first cycle capacity loss is directly proportional to delithiation rate, increasing from 9% at a C/10 rate to 27% at a 1C rate (Figure 3a). The increased 1^{st} cycle capacity loss at higher rates is clearly associated with an increase in the amount of trapped LiAl, as evidenced by the greater size and number of LiAl regions at a 2C delithiation rate compared to a C/10 rate (Figures 1c and 3d). A similar study was conducted with different areal capacities ranging from 1.0 mAh cm^{-2} to 7.5 mAh cm^{-2}, the latter being about twice the loading typically used in commercial cells (Figure 3b,e,f and S3). The theoretical capacity of the 40 μm foil is ~ 10.7 mAh cm^{-2}, leaving at least 10 μm of unreacted Al to act as a current collector. The current density was maintained at 0.67 mA cm^{-2}, so the rate was varied between 0.09C to 0.67C. The first cycle capacity loss is directly proportional to areal loading, increasing

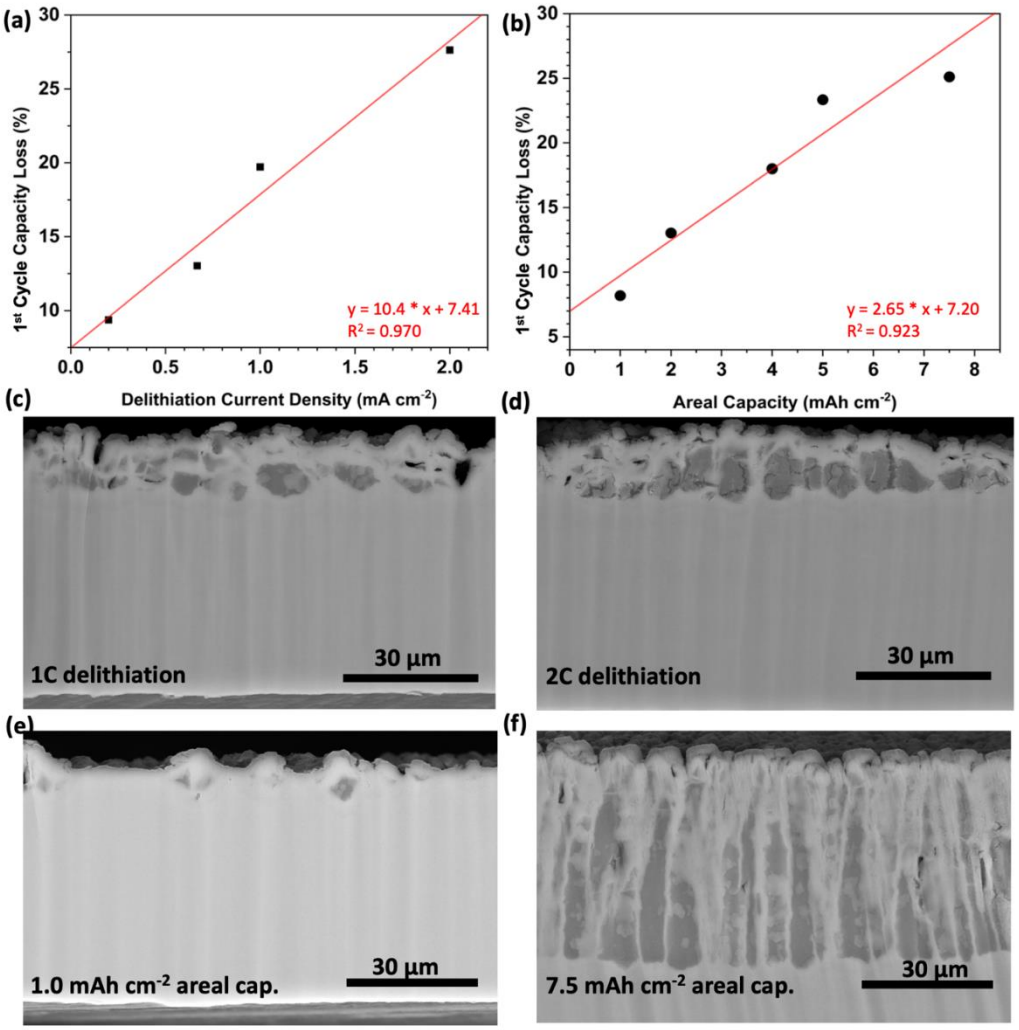

Figure 3: Effects of delithiation rate and areal capacity on the first cycle efficiency of aluminum foil anodes. **(a)** 1st cycle capacity loss versus delithiation current density, with an areal capacity of 2.0 mAh cm^{-2} and a delithiation current density ranging from 0.2 – 4.0 mA cm^{-2}. **(b)** 1st cycle capacity loss versus areal capacity, with a delithiation current density of 0.67 mA cm^{-2} and an areal capacity ranging from 1.0 – 7.5 mAh cm^{-2}. **(c,d)** BEIs taken after one cycle at an areal capacity of 2.0 mAh cm^{-2}, with delithiation rates of **(c)** 1C (2.0 mA cm^{-2}) and **(d)** 2C (4.0 mA cm^{-2}). **(e,f)** BEIs taken after one cycle at a current of 0.67 mA cm^{-2}, with an areal capacity of **(e)** 1.0 mAh cm^{-2} and **(f)** 7.5 mAh cm^{-2}.

from 8% at 1.0 mAh cm^{-2} to 25% at 7.5 mAh cm^{-2} (Figure 3b). This increased first cycle capacity loss at higher areal loading is also clearly associated with diffusional trapping. For the foil cycled at 7.5 mAh cm^{-2}, the grains are fully delithiated at the foil surface and yet mostly unreacted in the interior of the foil (Figure 3f).

The LiAl grain morphology after lithiation is similar regardless of areal capacity, maintaining a columnar structure with a grain width of 5 – 10 μm, and a length that is proportional to the areal capacity. This shows that for lithiation, the high lithium diffusivity of β-LiAl combined with the vertically oriented grain boundaries allows for facile lithiation kinetics, even at high areal capacity.[35] The dependence of first cycle capacity loss on delithiation rate and areal capacity can be explained in terms of the competition between delithiation at the grain boundaries versus the foil surface. At low rate and/or areal capacity, the grain boundaries can supply the necessary diffusion flux, so the delithiation reaction occurs primary at the β-LiAl grain boundaries (which have pre-existing α-Al) rather than at the foil surface. At high rate and/or areal capacity, insufficient diffusion flux limits the reaction rate at grain boundaries, which leads to nucleation and growth of α-Al at the foil surface. Once the Al surface layer becomes continuous, the rapid diffusion pathways along grain boundaries are disrupted, and the residual LiAl becomes kinetically isolated from the electrolyte. Thus, as the rate or areal capacity is increased, the fraction of the capacity, which is accessible before the surface passivates with Al will decrease. It is worth noting that while maintaining a practical cycling rate (e.g., C/3), increasing the areal capacity will also proportionally increase the current density, further exacerbating the diffusional lithium trapping. Considering the significant role of grain boundaries on both α-Al nucleation and lithium diffusion, it is expected that the LiAl grain structure after the initial lithiation will be a critical determinant of the diffusional trapping behavior. For example, a reduction in the grain width would yield a higher density of grain boundaries, which would both increase the effective diffusivity along the thickness of the foil and reduce the diffusion the path length within each grain.

The cycle life of aluminum foil anodes also depends significantly on both delithiation rate and areal capacity. At a C/10 rate, after 5 cycles, the capacity is relatively stable without much

fade during cycling, showing that diffusional trapping and mechanical degradation can be suppressed at sufficiently low rate and loading (Figure 4a). The cycle life decreases significantly at higher rates, from 81% retained capacity after 10 cycles at a C/10 rate to 42% at a 1C rate. Despite the large difference in cycle life between C/10 and C/3 rates, after one cycle, there is not a significant difference in mechanical degradation observed through SEM (Figures 1c and 2e). However, as the delithiation rate is increased to 1C or higher, there is an increase in mechanical degradation after one cycle, as evidenced by the internal cracking of the LiAl regions (Figure 3c-d). Compared to the delithiation rate, the areal capacity has a much larger effect on cycle life. After 10 cycles at 0.67 mA cm^{-2}, the foil lithiated to 2.0 mAh cm^{-2} retains 56% capacity, while the foil lithiated to 7.5 mAh cm^{-2} retains only 7% capacity (Figure 4b). As previously discussed, diffusional lithium trapping and mechanical degradation both contribute to the capacity fade during cycling. These observations suggest that diffusional trapping is the dominant mechanism of capacity fade in the first few cycles, especially at high areal loadings. However, it is likely that during extended cycling (e.g., > 10 cycles), mechanical degradation becomes the more significant source of capacity fade, especially at higher rates. For example, during the 10^{th} cycle at an initial areal capacity of 7.5 mAh cm^{-2}, the lithiation capacity is 1.1 mAh cm^{-2} and the columbic efficiency is 71%, compared to a 1^{st} cycle efficiency of 91% for a foil lithiated to 1.0 mAh cm^{-2}. This large difference in columbic efficiency can generally be explained by accelerated mechanical degradation after extended cycling, as is commonly observed in alloy anodes.[7]

The pulverization resulting from large volume change during alloying/dealloying contributes to several failure mechanisms, including loss of lithium inventory from SEI growth, or

loss of active material due to electronic isolation or disruption of solid-state diffusion pathways.[15,34,40] This mechanical degradation is evident from the embrittlement of the foils after cycling; after only 10 cycles, it becomes highly challenging to cross section and image the foils without breaking them. To qualitatively understand the extent of mechanical degradation in cycled

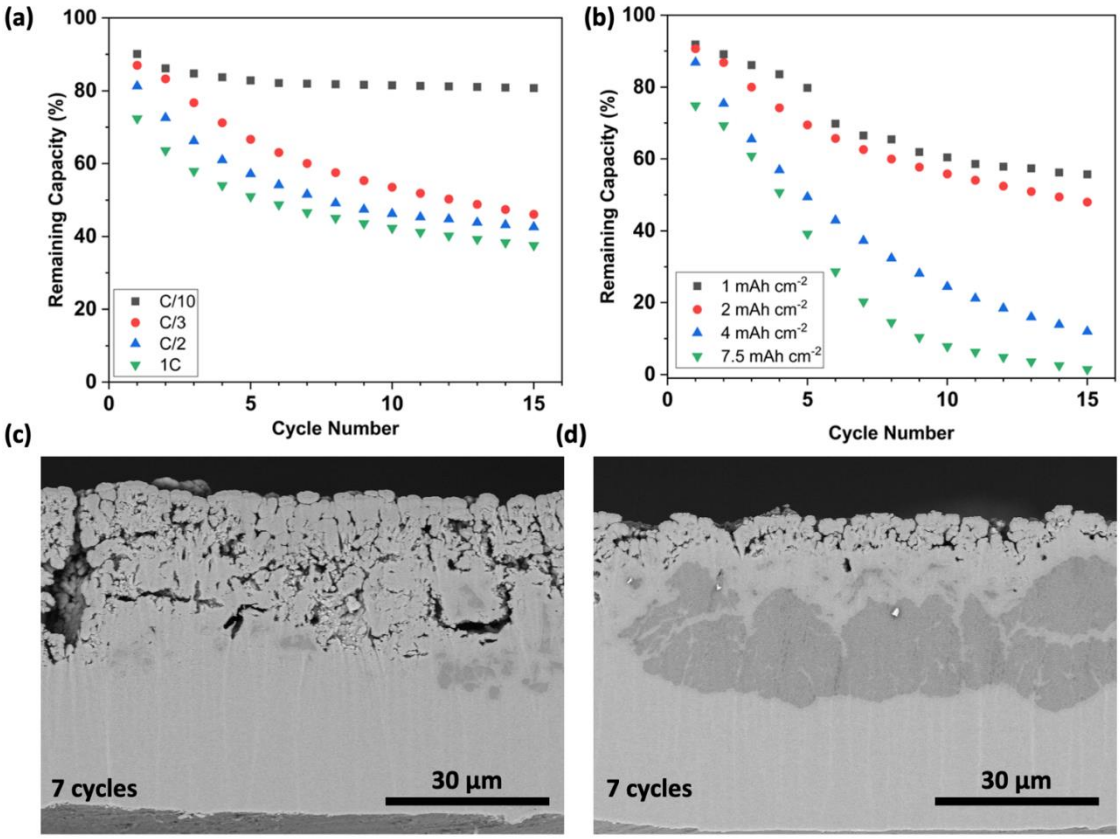

Figure 4: Effects of cycling rate and areal capacity on the cycle life of aluminum foil anodes. **(a)** LLI cycling data for Al foil anodes with initial areal capacity of 2.0 mAh cm^{-2} and cycling rate varying between C/10 to 1C. **(b)** LLI cycling data for Al foil anodes cycled at a current of 0.67 mA cm^{-2}, with initial areal capacity varying between 1.0 to 7.5 mAh cm^{-2}. **(c-d)** Representative cross-sectional BEIs of an Al foil after 7 cycles at a current density of 0.67 mA cm^{-2}, with an initial areal capacity of 2.0 mAh cm^{-2}.

foils, cross section BEIs were taken after 7 cycles for a foil cycled to 2.0 mAh cm^{-2} at 0.67 mA cm^{-2} (Figure 4c-d). It is apparent that both mechanical degradation and diffusional lithium trapping are responsible for the capacity fade, and that there is significant heterogeneity in the degradation mechanism of the foil. There are large regions (> 100 µm wide) where there is significant

pulverization of the foil and only small amounts of trapped LiAl. Conversely, there are also regions with minimal pulverization, but large regions of trapped LiAl. Considering that heterogeneity on the size scale of single grains (~ 10 μm) is observed after the first delithiation, it is not surprising that similar heterogeneity also manifests at larger size scales upon further cycling. It is plausible that heterogeneity in the LiAl grain structure affects the diffusion kinetics, which makes diffusional lithium trapping more severe in some regions than in others. In regions with more severe diffusional trapping, the foil may locally cycle at lower areal capacity and/or rate, which is expected to mitigate mechanical degradation. Conversely, in areas with less diffusional trapping, the foil will locally cycle at higher areal capacity and/or rate, which will exacerbate the mechanical degradation. The resulting pulverization of the foil then reduces the solid-state diffusion path length and locally mitigates the diffusional trapping. Clearly, the connection between diffusional lithium trapping of LiAl and the mechanical pulverization of active material in aluminum foil anodes cannot be ignored, as has been previously discussed.[34,36] Further investigation is needed to understand the root causes of this heterogeneity, as well as the complex relationship between these two degradation mechanisms.[40]

3.3 Effects of alloying elements on diffusional lithium trapping

In an effort to overcome diffusional lithium trapping, we investigated whether this behavior can be affected by the addition of alloying elements to the aluminum foils. Pre-lithiation is a common strategy to improve the first cycle efficiency and cycle life of alloying anodes. However, the methods employed in the literature are often not commercially scalable, such as direct contact with Li metal or electrochemical pre-cycling.[33,38,41,42] Here we employed an aluminum alloy containing 3 wt% Li (Al-Li), which is air stable and can be processed analogous to pure Al foils. The specific capacity of lithium in the as-synthesized Al-Li foil is 116 mAh g^{-1}, corresponding to

1.25 mAh cm^{-2} for a 40 μm foil. It has been shown that inclusion of 1 wt.% silicon in aluminum foils (i.e., $Al_{99.0}Si_{1.0}$ (Al-Si)) can significantly improve the cycling stability, although this reduces the first cycle efficiency to < 75%.[4,43] Thus, aluminum foils with 2 wt% lithium and 1 wt% silicon were synthesized in an attempt to simultaneously improve cycle life and first cycle efficiency. The $Al_{97.0}Li_{2.0}Si_{1.0}$ (Al-Li-Si) foil has a capacity of 77 mAh g^{-1}, or 0.83 mAh cm^{-2} for a 40 μm foil.

This pre-stored capacity is not available upon delithiation of pristine foils up to 3.0 V vs. Li/Li^+, which can be attributed to the poor lithium diffusivity of α-Al. However, upon the α-Al → β-LiAl phase transformation, this Li included in the a-Al phase becomes accessible, as evidenced by the extremely high first cycle efficiency of 101.3% for Al-Li, compared to 90.1% for pure Al (Figure 5a). This corresponds to a capacity of 110 mAh g^{-1} with respect to the mass of Al having undergone the phase transformation, which agrees well with the theoretical value. SEM reveals that after one cycle, there is still some LiAl trapped in the Al-Li foil, and the morphology is similar to the pure Al foil (Figure 5c,e). It appears that there is no fundamental difference in the diffusional trapping behavior of these two foils in the first cycle, but the inclusion of lithium in the foil mitigates the first cycle capacity loss from diffusional trapping. The cycle life of Al-Li is substantially better than Al, which can be attributed to the excess lithium inventory, which provides up to an additional 1.25 mAh cm^{-2} of capacity (Figure 5b). It is likely that only a fraction of this lithium is accessible since the majority (~ 80%) of the foil should not undergo the α-Al → β-LiAl phase transformation. However, it is possible that lithium could be slowly released from α-

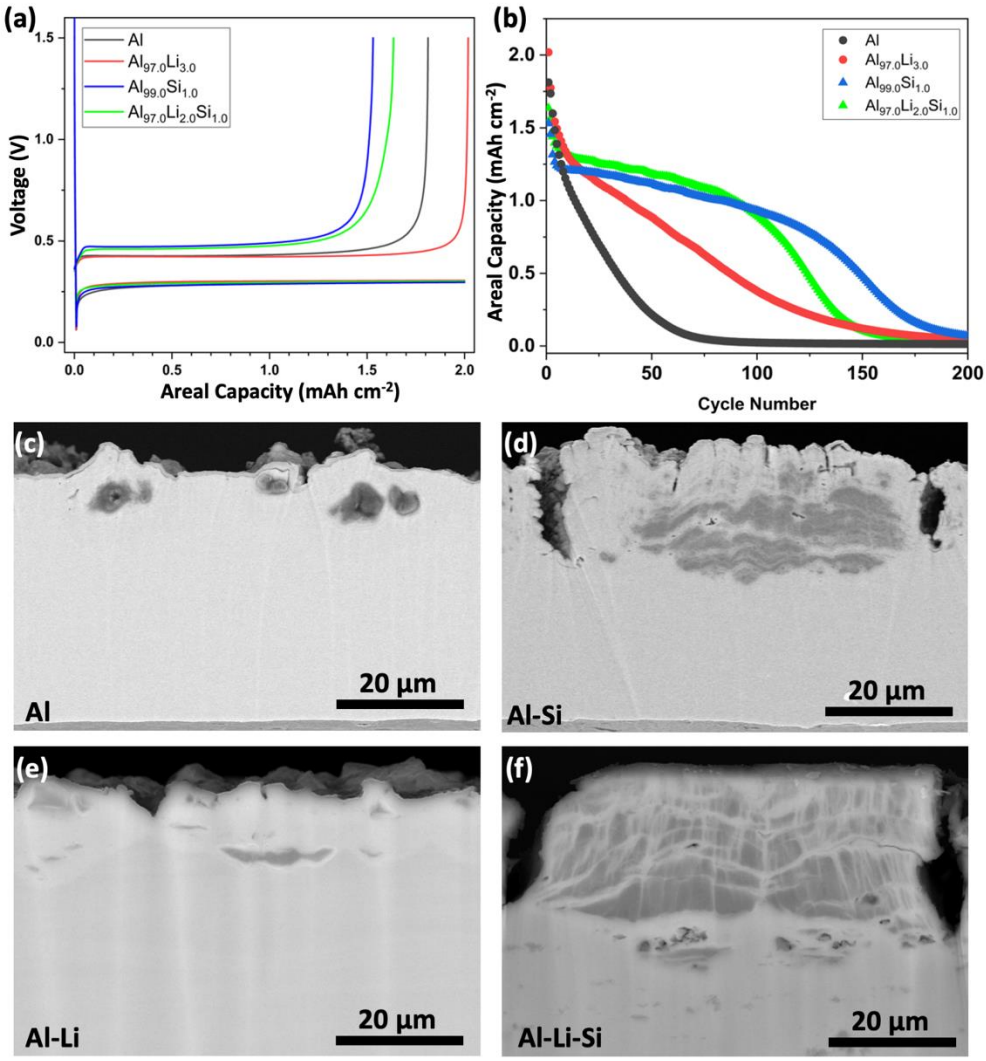

Figure 5: Electrochemical and post-mortem characterization of Al, Al-Si, Al-Li, and Al-Li-Si foils. **(a)** Voltage versus capacity plots for the first cycle at a C/10 rate with a lithiation capacity of 2.0 mAh cm^{-2}. **(b)** LLI cycling data for foil anodes cycled at a C/3 rate. **(c-f)** Cross-sectional BEIs of **(c)** Al, **(d)** Al-Si, **(e)** Al-Li, and **(f)** Al-Li-Si foils taken after one cycle at a C/10 rate, with an areal capacity of 2.0 mAh cm^{-2}.

Al during cycling, and there may also be differences in the foil morphology during cycling, which affect mechanical degradation or diffusion trapping.

The Al-Si foil has significantly lower 1st cycle efficiency of 76.4%, consistent with previous work, which is improved slightly to 81.7% with Al-Li-Si (Figure 5a). SEM images clearly show that diffusional lithium trapping is largely responsible for this low first cycle efficiency of

both Si-containing foils, as large regions of LiAl are observed under the foil surface (Figure 5d,f). Surprisingly, the LiAl grain structure after the 1st delithiation is completely different with 1% silicon addition. It is known that small amounts of alloying elements can significantly alter the grain structure of aluminum, and it is plausible that the grain structure of the pristine foil affects the grain structure of LiAl after electrochemical alloying.[44] Rather than the regularly sized, columnar LiAl grains observed in pure Al foils, the LiAl grain boundaries are instead primarily oriented parallel to the surface of the foil. The increased diffusional trapping of Si-containing Al foils can largely be explained by the lower density of vertically oriented LiAl grain boundaries, which provide rapid diffusion pathways through the thickness of the foil. The mechanical degradation is also different in the Si-containing foils, which exhibit much wider "mud cracks" with larger spacing between cracks, compared to the pure Al foil. Despite the lower 1st cycle efficiency, both Si-containing foils exhibit significantly better cycle life, which has been attributed to a reduction in mechanical degradation resulting from this different crack morphology.[12] However, it is also possible that the higher amount of trapped LiAl may slowly release Li during cycling, mitigating capacity fade due to loss of lithium inventory, as evidenced by the higher columbic efficiency of the Si-containing foils (Figure S4). A more detailed investigation of the relationship between the grain morphology of pristine versus lithiated foils, and how this is affected by alloying elements, would be highly valuable. By optimization of grain structure through alloying, it may be possible to simultaneously mitigate the mechanical degradation and diffusional lithium trapping in aluminum foil anodes.

Chapter 4: Conclusions

The objectives of this thesis were to determine diffusional lithium trapping to be a failure mechanism of aluminum foil anodes, to understand how this mechanism impacts the cycle life of aluminum foil anodes under practical cycling conditions, and to begin to overcome this issue in order to enable the use of aluminum anodes in lithium-ion batteries. Aluminum foil anodes have the promise to simultaneously improve the energy density and sustainability of LIBs at a lower cost, but their failure mechanisms need to be understood and overcome before they can be implemented in commercial cells. In this work, we demonstrated that kinetic trapping of β-LiAl is a significant source of capacity fade in aluminum foil anodes with a combination of LLI electrochemical cycling, XRD analysis, and *ex-situ* cross-sectional backscattered electron imaging. By analyzing BEIs of a single delithiation step, this trapping effect was found to be caused by the passivation of β-LiAl by an α-Al layer that grows initially at the grain boundaries, then eventually passivates the foil surface, kinetically isolating the β-LiAl from the electrolyte. This failure mechanism was found to be exacerbated by an increase in both the delithiation current density and areal capacity of the foil electrodes. While significant mechanical degradation of the foils is also observed, it appears that there is a complex interplay between diffusional lithium trapping and mechanical pulverization, which depends on the LiAl grain morphology. A new class of lithium-containing aluminum anodes was also investigated with electrochemical cycling and *ex-situ* cross-sectional BEI. The inclusion of lithium in the pristine foils yielded air-stable electrode materials ($Al_{97.0}Li_{3.0}$ and $Al_{97.0}Li_{2.0}Si_{1.0}$) that significantly increase the first cycle CE above their non-lithium-containing counterparts (Al and $Al_{99.0}Si_{1.0}$). Alloy design is a promising solution to both pulverization and diffusional trapping, and it offers a wide compositional space, which remains largely unexplored. The results reveal diffusional lithium trapping as a significant failure

mechanism of aluminum foil anodes and point towards the exploration of practically relevant strategies to overcome it. The work presented in this thesis provides a thorough understanding of diffusional lithium trapping in aluminum foil anodes with the hope that future research will overcome the poor cycle life of this material, and enable their adoption as a sustainable anode material for lithium-ion batteries.

Appendix: List of Publications

1. S.S. Sharma, **P.J. Crowley** and A. Manthiram, "Aluminum-Silicon Alloy Foils as Low-Cost, Environmentally Friendly Anodes for Lithium-ion Batteries." *ACS Sustainable Chemistry & Engineering*, **9**, 14515-14524 (2021).

2. **P.J. Crowley**, K. Scanlan and A. Manthiram, "Diffusional lithium trapping as a failure mechanism of aluminum foil anodes in lithium-ion batteries" Submitted to *Journal of Power Sources*.

References

[1] A. Manthiram, A reflection on lithium-ion battery cathode chemistry, Nat. Commun. 11 (2020) 1–9. https://doi.org/10.1038/s41467-020-15355-0.

[2] D. Larcher, J.M. Tarascon, Towards greener and more sustainable batteries for electrical energy storage, Nat. Chem. 7 (2015) 19–29. https://doi.org/10.1038/nchem.2085.

[3] X. Yu, A. Manthiram, Sustainable Battery Materials for Next-Generation Electrical Energy Storage, Adv. Energy Sustain. Res. 2 (2021) 2000102. https://doi.org/10.1002/aesr.202000102.

[4] S.S. Sharma, A. Manthiram, Towards more environmentally and socially responsible batteries, Energy Environ. Sci. 13 (2020) 4087–4097. https://doi.org/10.1039/d0ee02511a.

[5] B.T. Heligman, K.J. Kreder, A. Manthiram, Zn-Sn Interdigitated Eutectic Alloy Anodes with High Volumetric Capacity for Lithium-Ion Batteries, Joule. 3 (2019) 1051–1063. https://doi.org/10.1016/j.joule.2019.01.005.

[6] J. Asenbauer, T. Eisenmann, M. Kuenzel, A. Kazzazi, Z. Chen, D. Bresser, The success story of graphite as a lithium-ion anode material-fundamentals, remaining challenges, and recent developments including silicon (oxide) composites, Sustain. Energy Fuels. 4 (2020) 5387–5416. https://doi.org/10.1039/d0se00175a.

[7] W.J. Zhang, A review of the electrochemical performance of alloy anodes for lithium-ion batteries, J. Power Sources. 196 (2011) 13–24. https://doi.org/10.1016/j.jpowsour.2010.07.020.

[8] M.N. Obrovac, V.L. Chevrier, Alloy negative electrodes for Li-ion batteries, Chem. Rev. 114 (2014) 11444–11502. https://doi.org/10.1021/cr500207g.

[9] B.T. Heligman, A. Manthiram, Elemental Foil Anodes for Lithium-Ion Batteries, ACS Energy Lett. (2021) 2666–2672. https://doi.org/10.1021/acsenergylett.1c01145.

[10] H. Wang, H. Tan, X. Luo, H. Wang, T. Ma, M. Lv, X. Song, S. Jin, X. Chang, X. Li, The progress on aluminum-based anode materials for lithium-ion batteries, J. Mater. Chem. A. 8 (2020) 25649–25662. https://doi.org/10.1039/d0ta09762d.

[11] E. L. Bray, 2017 Minerals Yearbook: Aluminum; U.S. Geological Survey, 2020

[12] S.S. Sharma, P.J. Crowley, A. Manthiram, Aluminum-Silicon Alloy Foils as Low-Cost, Environmentally Friendly Anodes for Lithium-Ion Batteries, ACS Sustain. Chem. Eng. 9 (2021) 14515–14524. https://doi.org/10.1021/acssuschemeng.1c05168.

[13] D.H.S. Tan, Y.T. Chen, H. Yang, W. Bao, B. Sreenarayanan, J.M. Doux, W. Li, B. Lu, S.Y. Ham, B. Sayahpour, J. Scharf, E.A. Wu, G. Deysher, H.E. Han, H.J. Hah, H. Jeong, J.B. Lee, Z. Chen, Y.S. Meng, Carbon-free high-loading silicon anodes enabled by sulfide solid electrolytes, Science (80-.). 373 (2021) 1494–1499. https://doi.org/10.1126/science.abg7217.

[14] B.T. Heligman, K.P. Scanlan, A. Manthiram, An In-Depth Analysis of the Transformation of Tin Foil Anodes during Electrochemical Cycling in Lithium-Ion Batteries, J. Electrochem. Soc. 168 (2021) 120544. https://doi.org/10.1149/1945-7111/ac42f0.

[15] Y. Liu, N.S. Hudak, D.L. Huber, S.J. Limmer, J.P. Sullivan, J.Y. Huang, In situ transmission electron microscopy observation of pulverization of aluminum nanowires and evolution of the thin surface Al2O3 layers during lithiation-delithiation cycles, Nano Lett. 11 (2011) 4188–4194. https://doi.org/10.1021/nl202088h.

[16] B. Zhu, G. Liu, G. Lv, Y. Mu, Y. Zhao, Y. Wang, X. Li, P. Yao, Y. Deng, Y. Cui, J. Zhu, Minimized lithium trapping by isovalent isomorphism for high initial Coulombic efficiency of silicon anodes, Sci. Adv. 36 (2019) 1–9. https://doi.org/10.3866/PKU.WHXB201912010.

[17] H. Li, T. Yamaguchi, S. Matsumoto, H. Hoshikawa, T. Kumagai, N.L. Okamoto, T. Ichitsubo, Circumventing huge volume strain in alloy anodes of lithium batteries, Nat. Commun. (n.d.) 1–8. https://doi.org/10.1038/s41467-020-15452-0.

[18] P. Li, Y. Zhao, Y. Shen, S. Bo, Fracture behavior in battery materials, J. Phys. Energy. (2020) 0–28.

[19] K.J. Kreder, B.T. Heligman, A. Manthiram, Interdigitated Eutectic Alloy Foil Anodes for Rechargeable Batteries, ACS Energy Lett. 2 (2017) 2422–2423. https://doi.org/10.1021/acsenergylett.7b00844.

[20] B.T. Heligman, K.P. Scanlan, A. Manthiram, Nanostructured Composite Foils Produced Via Accumulative Roll Bonding as Lithium-Ion Battery Anodes, ACS Appl. Mater. Interfaces. 14 (2022) 11408–11414. https://doi.org/10.1021/acsami.1c23529.

[21] N. Liu, H. Wu, M.T. McDowell, Y. Yao, C. Wang, Y. Cui, A yolk-shell design for stabilized and scalable Li-ion battery alloy anodes, Nano Lett. 12 (2012) 3315–3321. https://doi.org/10.1021/nl3014814.

[22] B. Ji, F. Zhang, M. Sheng, X. Tong, Y. Tang, A Novel and Generalized Lithium-Ion-Battery Configuration utilizing Al Foil as Both Anode and Current Collector for Enhanced Energy Density, Adv. Mater. 29 (2017) 1–7. https://doi.org/10.1002/adma.201604219.

[23] D. Rehnlund, F. Lindgren, S. Böhme, T. Nordh, Y. Zou, J. Pettersson, U. Bexell, M. Boman, K. Edström, L. Nyholm, Lithium trapping in alloy forming electrodes and current collectors for lithium based batteries, Energy Environ. Sci. 10 (2017) 1350–1357. https://doi.org/10.1039/c7ee00244k.

[24] D. Rehnlund, Z. Wang, L. Nyholm, Lithium-Diffusion Induced Capacity Losses in Lithium-Based Batteries, Adv. Mater. 34 (2022) 2108827. https://doi.org/10.1002/adma.202108827.

[25] J.R. Owen, W.C. Maskell, B.C.H. Steele, T.S. Nielsen, O.T. Sørensen, Thin film lithium aluminium negative plate material, Solid State Ionics. 13 (1984) 329–334. https://doi.org/10.1016/0167-2738(84)90076-6.

[26] Y. Geronov, P. Zlatilova, G. Staikov, The secondary lithium-aluminium electrode at room temperature. II. Kinetics of the electrochemical formation of the lithium-aluminium alloy, J. Power Sources. 12 (1984) 155–165. https://doi.org/10.1016/0378-7753(84)80046-4.

[27] T.R. Jow, C.C. Liang, Lithium-Aluminum Electrodes at Ambient Temperatures, J. Electrochem. Soc. 129 (1982) 1429–1434. https://doi.org/10.1149/1.2124178.

[28] A.S. Baranski, W.R. Fawcett, The Formation of Lithium-Aluminum Alloys at an Aluminum Electrode in Propylene Carbonate, J. Electrochem. Soc. 129 (1982) 901–907. https://doi.org/10.1149/1.2124050.

[29] G. Oltean, C.W. Tai, K. Edström, L. Nyholm, On the origin of the capacity fading for aluminium negative electrodes in Li-ion batteries, J. Power Sources. 269 (2014) 266–273. https://doi.org/10.1016/j.jpowsour.2014.06.118.

[30] N.S. Hudak, D.L. Huber, Size Effects in the Electrochemical Alloying and Cycling of Electrodeposited Aluminum with Lithium, J. Electrochem. Soc. 159 (2012) A688–A695. https://doi.org/10.1149/2.023206jes.

[31] D.X. Liu, A.C. Co, Revealing Chemical Processes Involved in Electrochemical (De)Lithiation of Al with in Situ Neutron Depth Profiling and X-ray Diffraction, J. Am. Chem. Soc. 138 (2016) 231–238. https://doi.org/10.1021/jacs.5b10295.

[32] M.S. Leite, D. Ruzmetov, Z. Li, L.A. Bendersky, N.C. Bartelt, A. Kolmakov, A.A. Talin, Insights into capacity loss mechanisms of all-solid-state Li-ion batteries with Al anodes, J. Mater. Chem. A. 2 (2014) 20552–20559. https://doi.org/10.1039/c4ta03716b.

[33] Y. Yu, S. Li, H. Fan, H. Xu, M. Jiang, Y. Huang, J. Li, Optimal annealing of Al foil anode for prelithiation and full-cell cycling in Li-ion battery: The role of grain boundaries in lithiation/delithiation ductility, Nano Energy. 67 (2020). https://doi.org/10.1016/j.nanoen.2019.104274.

[34] T. Zheng, D. Kramer, M.H. Tahmasebi, R. Mönig, S.T. Boles, Exploring the Reversibility of Phase Transformations in Aluminum Anodes through Operando Light Microscopy and Stress Analysis, ChemSusChem. 13 (2020) 5910–5920. https://doi.org/10.1002/cssc.202002023.

[35] T. Zheng, X. Wang, E. Jain, D. Kramer, R. Mönig, M. Seita, S.T. Boles, Granular phase transformation of polycrystalline aluminum during electrochemical lithiation, Scr. Mater. 188 (2020) 164–168. https://doi.org/10.1016/j.scriptamat.2020.07.029.

[36] T. Zheng, D. Kramer, M.H. Tahmasebi, R. Mönig, S.T. Boles, Improvement of the Cycling Performance of Aluminum Anodes through Operando Light Microscopy and Kinetic Analysis, ChemSusChem. 13 (2020) 974–985. https://doi.org/10.1002/cssc.201903060.

[37] R. Rupp, B. Caerts, A. Vantomme, J. Fransaer, A. Vlad, J. Phys. Chem. Lett. 2019, 10, 5206.

[38] W.C. Maskell, J.R. Owen, Cycling Behavior of Thin Film LiAl Electrodes with Liquid and Solid Electrolytes, J. Electrochem. Soc. 132 (1985) 1602–1607. https://doi.org/10.1149/1.2114174.

[39] L.Y. Beaulieu, K.W. Eberman, R.L. Turner, L.J. Krause, J.R. Dahna, Colossal reversible volume changes in lithium alloys, Electrochem. Solid-State Lett. 4 (2001). https://doi.org/10.1149/1.1388178.

[40] Jiang, M., Yu, Y., Fan, H., Xu, H., Zheng, Y., Huang, Y., … Li, J. (2019). Full-Cell Cycling of a Self-Supporting Aluminum Foil Anode with a Phosphate Conversion Coating. *ACS Applied Materials and Interfaces*, *11*(17), 15656–15661. https://doi.org/10.1021/acsami.9b02813

[41] S. Chen, X. Yang, J. Zhang, J. Ma, Y. Meng, K. Tao, F. Li, J. Geng, Aluminum−lithium alloy as a stable and reversible anode for lithium batteries, Electrochim. Acta. 368 (2021) 137626. https://doi.org/10.1016/j.electacta.2020.137626.

[42] T. Zheng, D. Kramer, R. Mönig, S.T. Boles, Aluminum Foil Anodes for Li-Ion Rechargeable Batteries: The Role of Li Solubility within β-LiAl, ACS Sustain. Chem. Eng. 10 (2022) 3203–3210. https://doi.org/10.1021/acssuschemeng.1c07242.

[43] M.H. Tahmasebi, D. Kramer, H. Geßwein, T. Zheng, K.C. Leung, B.T.W. Lo, R. Mönig, S.T. Boles, In situ formation of aluminum-silicon-lithium active materials in aluminum matrices for lithium-ion batteries, J. Mater. Chem. A. 8 (2020) 4877–4888. https://doi.org/10.1039/c9ta13745a.

[44] RG Guan, D. Tie, A Review on Grain Refinement of Aluminum Alloys: Progress, Challenges and Prospects, Acta Metall. Sin. (Engl. Lett.) **30,** 409-432 (2017). https://doi.org/10.1007/s40195-017-0565-